Chemical Engineering Journal Advances 21 (2025) 100703

Contents lists available at ScienceDirect

Chemical Engineering Journal Advances

journal homepage: www.sciencedirect.com/journal/chemical-engineering-journal-advances

Response surface method-driven design of experiments for the synthesis of fly ash-based geopolymers in the gallic acid optimized removal from wastewater

Ana Paula Ferreira [a,b,*], Ana Paula S. Natal [a,c], Arthur P. Baldo [a,c], Adriano S. Silva [a,e,f], Jose L. Diaz de Tuesta [d], Pricila Marin [c], José A. Peres [b], Helder T. Gomes [a,*]

[a] CIMO, LA SusTEC, Instituto Politécnico de Bragança, Campus de Santa Apolónia, 5300- 253 Bragança, Portugal
[b] Chemistry Center of Vila Real (CQVR), University of Trás-os-Montes and Alto Douro, Quinta de Prados, 5000-801 Vila Real, Portugal
[c] Universidade Tecnológica Federal do Paraná (UTFPR), Campus Apucarana, 86812-460, Londrina, Brazil
[d] Chemical and Environmental Engineering Group, ESCET, Universidad Rey Juan Carlos, c/Tulipán s/n 28933 Móstoles, Spain
[e] ALiCE – Associate Laboratory in Chemical Engineering, Faculty of Engineering, University of Porto, Rua Dr. Roberto Frias, 4200- 11 465 Porto, Portugal
[f] Research Centre in Digitalization and Intelligent Robotics (CeDRI), Instituto Politécnico de Bragança, Campus de Santa Apolónia, 13 5300-253 Bragança, Portugal

ARTICLE INFO

Keywords:
Design of experiments
Box-Behnken design
Wastewater treatment
Phenolic compounds removal
Waste valorization
Fly-ash
Eco-friendly materials

ABSTRACT

The growing need for sustainable wastewater treatment solutions has led to exploring alternative materials to explore large-scale and reliable technologies. This study focuses on optimizing the synthesis of geopolymers based on fly ash using a Box-Behnken experimental design to enhance their adsorption efficiency for phenolic compounds, as gallic acid model pollutant which are widely found in wastewater leaching from landfills. Fifteen geopolymer samples were synthesized, characterized, and tested for adsorption performance. Various techniques were employed, including X-ray diffraction (XRD), scanning electron microscopy (SEM), Fourier transform infrared (FT-IR) spectroscopy. The optimization process highlighted the significance of the Si/Al mass ratio, NaOH molar concentration, and Na_2SiO_3/NaOH as variables in the geopolymers production. Geopolymer samples demonstrated significant adsorption capacities, with GP_2.0_10_2.5 achieving a maximum adsorption capacity of 75.8 mg g^{-1}. Kinetic studies indicated that the pseudo-first-order model best described the adsorption process. At the same time, equilibrium data fitted well with both Langmuir and Freundlich isotherms, with GP_2.0_10_2.5 showing the best fit for the Langmuir model. These findings reveal the potential of geopolymers derived from fly ash as cost-effective adsorbents in wastewater treatment, promoting the reuse of industrial waste within the framework of a Circular Economy.

1. Introduction

Population growth, rapid urbanization, and escalating consumption have collectively driven a substantial surge in solid waste production over the years [1]. Globally, the annual generation of municipal solid waste (MSW) has soared to 2.10 billion tons, with projections anticipating a staggering 3.40 billion tons by 2050. This trajectory underscores solid waste as a poignant symbol of inefficiency and resource misallocation in contemporary society, cementing its status as a pivotal environmental predicament [2]. In March 2020, the European Commission introduced an innovative Circular Economy (CE) action plan [3]. Its goal is to promote sustainable consumption by reducing resource losses and extending the use of resources in production cycles. These address rising landfill waste and lower the demand for virgin resources. Key strategies in the plan include embedding sustainability into product design and making products more durable, reusable, and recyclable while reducing carbon footprints. Additionally, circular production processes aim to cut energy use, raw material costs, and overall

Abbreviations: ANOVA, Analysis of variance; BBD, Box behnken design; CE, Circular economy; DOE, Design of Experiment; FA, Fly ash; FT-IR, Fourier transform infrared spectroscopy; GA, Gallic acid; GPs, Geopolymers; HPLC, High-performance liquid chromatography; ICP-OES, Inductively coupled plasma optical emission spectroscopy; MSW, Municipal solid waste; pH_{PZC}, Point of zero charge; E (%), Removal efficiency; RSM, Response surface methodology; SEM, Scanning electron microscopy; EDS, Energy dispersive spectroscopy; XRD, X-ray diffraction.

* Corresponding authors.
E-mail addresses: anapaula.silva@ipb.pt (A.P. Ferreira), htgomes@ipb.pt (H.T. Gomes).

https://doi.org/10.1016/j.ceja.2024.100703

Available online 7 January 2025

economic expenses [3].

By harnessing MSW as an alternative resource for product generation, as opposed to virgin raw materials, the proposed CE paradigm can effectively attenuate the predicament of mounting MSW volumes in landfills and concurrently preserve the environment from resource overexploitation [4]. The potential avenues for reincorporating MSW into the economic framework encompass conventional incineration [5], hydrothermal treatments [6], pyrolysis [7], and thermochemical and hydrothermal liquefaction [8]. Additionally, MSW offers a viable avenue for synthesizing inorganic materials, exemplified by creating geopolymers (GPs) [9]. GPs are ceramic materials engendered through geopolymerization reactions at low temperatures [10]. Their composition derives from diverse sources such as silica fume, nuclear waste [11], rice husk ash [12], natural fibers [13], waste glass [14], plastics [15], municipal solid incineration ash [16], and more [9]. Significantly, incinerated MSW ash, spanning both bottom and fly ash (FA), stands out as a prominent aluminosilicate resource for such synthesis [17]. The unique precursor composition invariably governs the ensuing structure and characteristics of GPs, thereby determining their applicability across a spectrum of domains encompassing aeronautical engineering [18], nuclear industry ventures [19], archaeological explorations [20], construction materials development [17], and their utility as water treatment adsorbents [21]. The literature is enriched with studies dealing with adsorption of ion metals such as copper [22], cesium [23], and heavy metals [24]. Yu et al., for example, achieved 95 % Cu(II) adsorption after five regeneration cycles [22], and Cheng et al. optimized pH and temperature for the adsorption of Pb^{2+}, Cu^{2+}, Cr^{3+}, and Cd^{2+} [24] Other papers have also explored heavy metal adsorption using GPs [25], and the process is often efficient due to the heavy metals' ion exchange with Na^{+} in the GP [24]. However, there is a lack of studies addressing the utilization of GPs as an adsorbent of phenolic compounds commonly found in polluted water streams from industrial and urban wastewater.

Phenolic compounds are present in several effluents, including industrial [26](*e.g.,* oil pesticides and herbicides production, pharmaceuticals, plastics, and textiles), agricultural [27], and urban wastewater [28]. These compounds can present adverse effects on the water ecosystem even at low concentrations [29], and treatment solutions are required to ensure that all phenolic-containing effluents are properly treated before discharging in water bodies. Among them, gallic acid (GA) is of particular concern due to its high reactivity and potential to disrupt aquatic environments [30]. Gallic acid (3,4,5-trihydroxybenzoic acid), given its molecular structure, is prone to interactions with other environmental contaminants and can contribute to the formation of more persistent compounds [31–33]. Furthermore, its antioxidant properties, while beneficial in controlled applications, can lead to oxidative stress in aquatic organisms when present in excess [34]. These characteristics make gallic acid an important model compound for studying phenolic pollutant adsorption.

In this regard, adsorption represents one interesting treatment option with mild operating conditions and low temperatures [35]. So far, carbonaceous materials are the most representative materials used for this purpose [36]. However, the synthesis procedure of carbon materials often involves the utilization of high temperatures, which can increase the synthesis cost. Despite the promising results achieved in this field of study, there remains a need for more sustainable and optimized materials to enhance process feasibility. For instance, the works of Jia X et all. [37], and Oyehan T. et all. [38], address fly ash valorization, exploring its use as spherical grains or grafted with an ultrathin film of polydiallyldimethyl ammonium for phenolic compound removal. In most cases, these studies focus on evaluating process parameters such as pH, concentration, and temperature. For example, [39] applied fly ash geopolymers for phenol removal. However, while these studies provide valuable insights, they do not apply advanced optimization techniques such as the Response Surface Methodology (RSM).

Therefore, this work used RSM to optimize GP synthesis, targeting the removal of GA from wastewater. To achieve this goal, Box Behnken Design (BBD) was used to evaluate the impact of different synthesis conditions on the capacity of the GP to adsorb GA, chosen as a model phenolic compound. This design uses a matrix with three levels (−1, 0, +1) for each independent variable, positioning points at the midpoints of the edges of the cubic design region and in the center. The setup generates data to model the response surface and fine-tune process parameters. Using 12 edge nodes and 3 center nodes to fit a second-order equation, the BBD resulted in 15 experiments, enabling optimization of the GP synthesis process for improved performance. Selected GPs were also characterized to correlate the synthesis procedure with physicochemical characteristics and adsorption performance. Additional effort was made to study the adsorption isotherms equilibrium fitness to Freundlich and Langmuir models; as well as studying the GA adsorption kinetics into GPs using the pseudo-first-order model and the pseudo-second-order model.

2. Methodology

2.1. Reagents and materials

For the production of GPs, the FA was provided by SOGAMA [40] (MSW management complex in Cerceda, Galicia, Spain), whose chemical composition determined by ICP-OES is in Table S1, aluminum oxide (Al_2O_3 - 99.7 %), provided by Thermo Scientific; sodium hydroxide pearls (NaOH - 98 %), provided by Labkem; sodium silicate (Na_2SiO_3: $Na_2O = 10.6$ % and $SiO_2 = 26.5$ %), provided by Fisher Chemical; were used. GA ($C_6H_2(OH)_3COOH$ – 98 %), provided by EMD Millipore Corporation, was used as a pollutant model of phenolic compounds for the adsorption and hydrochloric acid (HCl – 37 %), provided by VWR Chemicals was used to wash and neutralize the pH of the GPs. For HPLC analysis, phosphoric acid (H_3PO_4 - 85 %) and acetonitrile (C_2H_3N - 99 %), both provided by Fisher Scientific, were used. All reagents were used as received, and ultrapure water was used for solution preparation and washing procedures during this work.

2.2. Geopolymer synthesis and its optimization

The reactants, *viz.* FA, NaOH, Al_2O_3, and Na_2SiO_3 were uniformly mixed by hand, and the resulting homogenous paste was molded into cubic forms measuring 45 × 45 × 45 mm. The amounts of each reactant were defined according to a BBD arrangement. Three parameters previously identified to influence this process are considered: Si/Al mass ratio [41,42], NaOH molar concentration (M) [25,43], and Na_2SiO_3/-NaOH weight ratio [44,45]. Each factor was tested at three levels of component content: high (1), medium (0), and low (−1). The design places points on the midpoints of the edges of the cubic design region and points in the center to generate experimental data that can be used to model the response surface and optimize the process parameters. It utilizes the twelve center edge nodes and the three center nodes to fit a second-order equation, resulting in 15 experiments. Table S2 shows the ranges and experimental values of the independent variables considered for the design, and Figure S1 shows a scheme that represents this design.

The design was created and analyzed using R-Studio: 2023.09.1 + 494 Desktop Open-Source Edition (AGPL v3, 64-bit operating system), which was used for design conception, mathematical modeling, graphical and statistical treatment of the results, and optimization. It is a comprehensive, open-source, integrated development environment that supports statistical computing, data analysis, and visualization.

Accordingly, fifteen GPs were synthesized using the Design of Experiment (DOE) approach, with each sample utilizing an initial FA mass of 10 g, while varying in the Si/Al mass ratio (1.5, 2.0, and 2.5), NaOH molar concentration (5.0, 7.5 and 10 M) and Na_2SiO_3/NaOH (1.0, 1.75 and 2.5) mass ratio.

After uniformly mixed, the samples were then cured at 40 °C for 24 h in an oven. The GPs were first ground into a fine powder to facilitate

adsorption studies. Following this, the crushed GP was thoroughly washed several times using distilled water and a 0.1 M hydrochloric acid solution until the pH of the solution containing the GP was neutral (pH ≤ 7) (Figure S2). After washing, the GP was dried overnight at 40 °C. The dried GP was then sieved to isolate particles smaller than 53 μm. The nomenclature of each geopolymer is represented by the "GP" suffix followed by the composition values in the format GP_Si/Al_NaOH_NaSiO/NaOH. For example, GP_1.5_5.0_1.75 indicates a molar ratio of 1.5 for Si/Al, 5.0 for NaOH, and 1.75 for Na_2SiO_3/NaOH, corresponding to the proportions of the components used in the material's synthesis, this information can be confirmed in Table S2.

2.3. Characterization of the geopolymers

The chemical composition of FA was determined by inductively coupled plasma optical emission spectroscopy (ICP-OES) analysis using Vista AX Pro-720ES equipment.

The GPs were characterized using several analytical techniques. An adsorption analyzer (Quantachrome NOVATOUCH LX4) was used to determine the prepared adsorbent's surface area and pore volumes. The surface chemistry analysis for the GPs and FA was tracked using Fourier Transform Infrared Spectroscopy (FT-IR), utilizing a PerkinElmer FT-IR spectrophotometer UATR Two. X-ray diffraction (XRD) measurements were conducted at room temperature using a PANalytical X'Pert Pro diffractometer, which is equipped with an X'Celerator detector and a secondary monochromator in θ/2θ Bragg-Brentano geometry. To assess the material's acid-base properties, various solutions were prepared and titrated to determine acidic and basic sites. For acidic sites, the samples (0.2 g) were mixed with NaOH (0.02 mol l^{-1}) and then titrated with HCl (0.01 mol l^{-1}). For basic sites, the samples were mixed with HCl (0.02 mol l^{-1}) and then titrated with NaOH (0.01 mol l^{-1}). Acidic site concentration was determined by the moles of NaOH consumed, while basic site concentration was determined by the moles of HCl consumed, both normalized to the sample mass. The following Eq. (1 and 2) was used for sites calculations:

$$C_{acidic} = \frac{C_{NaOH} \cdot V_{NaOH} - C_{HCl} \cdot V_{HCl}}{m_{sample}} \quad (1)$$

$$C_{basic} = \frac{C_{HCl} \cdot V_{HCl} - C_{NaOH} \cdot V_{NaOH}}{m_{sample}} \quad (2)$$

Where C_{acidic} and C_{basic} (mmol g^{-1}) represents the concentration of acidic or basic sites on geopolymer's surface, C_{NaOH} and C_{HCl} (mol L^{-1}) are the initial concentrations of NaOH and HCl, respectively, V_{NaOH} (L) is the volume of NaOH added during titration, V_{HCl} (L) is the volume of HCl added during titration, and m_{sample} (g) is the mass of the solid sample used.

To determine the point of zero charge (pH_{PZC}), nine dilutions of NaCl (0.01 mol L^{-1}) were prepared, and their pH was adjusted between 4 and 12 by adding NaOH (0.02 mol l^{-1}) or HCl (0.02 mol l^{-1}). To study pH effects on the material's adsorption performance, 0.15 g of the solid sample was added to each solution and stirred at 300 rpm and 25 °C for 1440 min. After filtration, the pH of the solutions was measured, and the final and initial pH values were plotted to determine the pH at which the surface charge of the adsorbent is zero.

Scanning electron microscopy combined with energy dispersive spectroscopy (SEM/EDS) was conducted to investigate the morphological and microstructural features of the precursor material and GP. The samples were analyzed using a FEI Quanta 400 SEM with a resolution of 4 nm, equipped with an Everhart-Thornley detector for backscattered and secondary electron contrast.

2.4. Adsorption runs

Each GP [2.5 g l^{-1}] sample was introduced into the GA solution [50 mg l^{-1}]. The solution underwent agitation on a magnetic stirrer at 300 rpm, with a consistent temperature of 50 °C, sustained for 480 min. Aliquots were collected from the vessel at eight distinct time intervals (0, 15, 30, 60, 120, 240, 360, and 480 min) to monitor chemical compound concentration during the experiment.

Adsorption capacity q_t (mg g^{-1}) was determined with Eq. (3), while the GPs' removal efficiency E (%) was calculated using Eq. (4).

$$q_t = \frac{(C_0 - C_t) \times V}{m} \quad (3)$$

$$E = \frac{(C_0 - C_t)}{C_0} \times 100\% \quad (4)$$

Where C_0 (mg l^{-1}) is the initial concentration of the pollutant (phenolic compound), C_t (mg l^{-1}) is the concentration of the pollutant in the liquid phase at a time t (min), V (L) is the volume of the pollutant solution, and m (g) is the mass of adsorbent.

High-performance liquid chromatography (HPLC) with a UV–Vis spectrophotometer detector (JASCO HPLC system, UV – 2075 Plus, PU-2089 Plus and LC—NETII/ADC) was employed to determine the amount of gallic acid in aliquots obtained from the adsorption tests. For the analysis, an Ultra BiPh column (*RESTEK* - 5 μm, 150 mm × 2.1 mm) and a mobile phase consisting of 95 % phosphoric acid and 5 % acetonitrile were used. The system operated isocratically at a flow rate of 0.3 mL/min, with gallic acid detection performed at a wavelength of 277 nm.

2.5. Calculation methods

2.5.1. Response surface methodology

The RSM is a proper experimental design that applies statistical and mathematical techniques to optimize the investigated variables. Specifically, the BBD, a type of RSM, is used to study the effects of independent variables (x_1, x_2, …, x_n) and their interactions. The goal is to find the relationships between these variables and the system's response (y_1, y_2, …, y_n) through a quadratic polynomial Eq. (5).

$$y = \beta_0 + \Sigma_{i=1}^{k}\beta_i x_i + \Sigma_{i=1}^{k}\beta_{ii}x_i^2 + \Sigma_{i=1}^{k-1}\beta_{ij}x_i x_j + \varepsilon \quad (5)$$

Where y is the output response, β is the regression coefficient estimated from the experimental data, k is the number of experimental parameters, xi, and xj are the variables that represent the evaluated parameters and ε is the random error [46]. In this work, the identified parameters were x_1 (Si/Al ratio), x_2 (NaOH concentration), and x_3 (Na_2SiO_3/NaOH ratio). The recorded response value was the removal efficiency (E%), denoted as y_1. The Solver tool in Microsoft ® Excel and which employs the Generalized Reduced Gradient algorithm, was used to estimate the coefficients by multiple non-linear regression. The analysis of variance (ANOVA) was used to evaluate both the coefficients' statistical significance and the fitting of the function [46]. The objective functions were maximized or minimized, as appropriate, using as restrictions the minimum and maximum values of the operating variables provided in Table S2.

2.5.2. Equilibrium isotherms models

Two commonly used isotherms for solid-liquid systems will be evaluated: Langmuir and Freundlich[23]. Eq. (6) gives the expression representing this model.

$$q_e = \frac{q_m K_L C_e}{1 + K_L C_e} \quad (6)$$

where q_m is the maximum adsorption capacity of the adsorbent (mg g^{-1}), C_e is the GA equilibrium concentration at equilibrium (mg l^{-1}), and K_L is the Langmuir adsorption constant (L mg^{-1}).

In contrast, the Freundlich isotherm model is interpreted as a model for sorption onto a heterogeneous surface that contains sites with varying affinities[24]. Eq. (7) shows how this model is represented.

$$q_{eq} = K_F C_{eq}^{1/n_F} \quad (7)$$

K_F is the Freundlich constant (L g^{-1}), and n_F is the dimensionless Freundlich constant related to the intensity of adsorption, values in the range 1 to 10 represent favorable adsorption conditions.

2.5.3. Kinetic modeling

This study employed three kinetic models: the pseudo-first-order model, the pseudo-second-order, and the intraparticle diffusion model. The mathematical expression is given by Eqs. (8), (9), and (10) [47].

$$q_t = q_e\left(1 - e^{-k_1 t}\right) \quad (8)$$

$$q_t = \frac{q_e^2 k_2 t}{1 + q_e k_2 t} \quad (9)$$

$$q_t = k_{id} t^{1/2} + I \quad (10)$$

q_e is the adsorption capacity at equilibrium (mg g^{-1}), k_1 is the adsorption rate kinetic constant of the pseudo-first-order model (min^{-1}), k_2 is the adsorption rate kinetic constant of the pseudo-second-order model (g mg^{-1} min^{-1}), and k_{id} is the intraparticle diffusion rate constant (mg g^{-1} $min^{-0.5}$), and I is the intercept (mg g^{-1}).

3. Results and discussion

Five samples of prepared GPs were selected for the characterization to ensure balanced coverage of critical points within the experimental space. The selection included GP_2.0_7.5_1.75, representing the central point of the experimental design, as well as, GP_2.0_10_2.5, GP_1.5_10_1.75, GP_1.5_7.5_1.0, and GP_2.5_5.0_1.75, which were carefully chosen to capture the maximum and minimum variation of key parameters, such as molar ratios and concentrations. Also, it included the most effective formulations in GA removal. This approach ensures that different zones of the BBD are investigated, providing a comprehensive view of the GP properties.

3.1. Characterization

3.1.1. Textural properties

Table 1 presents the textural properties results for FA and GP_2.0_7.5_1.75, GP_2.0_10_2.5, GP_1.5_10_1.75, GP_1.5_7.5_1.0, and GP_2.5_5.0_1.75. The data shows a significant increase in the surface area of all the GPs compared to the precursor material, attributed to their higher porosity. Moreover, the geopolymerization process led to an increase in the total pore volume, indicating the role of this process in enhancing pore formation within the GP matrix [48]. It is worth noting that the average pore size of the GPs generally did not show significant changes compared to the FA. However, GP_2.5_5.0_1.75 exhibited a total pore volume of 0.123 cm^3 g^{-1}, notably different from the other GPs and the other analyzed parameters.

The surface area results for GP_2.0_7.5_1.75, GP_2.0_10_2.5, GP_1.5_10_1.75, and GP_1.5_7.5_1.0 are comparable to those shown by Syial et al. [48], who produced a GP using FA (SiO_2 - 43.25 wt.% and Al_2O_3 - 20.58 wt.%) from a local coal-fired power plant in Manjung, Perak, Malaysia. The surface area obtained in that study was 31 m^2 g^{-1}, while in this study, it was found to be 35 m^2 g^{-1} for GP_2.0_7.5_1.75, 61 m^2/g for GP_2.5_5.0_1.75 and 30 m^2 g^{-1} for the other GPs.

Table 1
Textural properties analysis of FA and GPs adsorbents.

Sample	S_{BET} (m^2 g^{-1})	$S_{Langmuir}$ (m^2 g^{-1})	S_{ext} (m^2 g^{-1})	V_{total} (cm^3 g^{-1})
FA	13	248	1	0.015
GP_2.0_7.5_1.75	35	267	7	0.074
GP_2.0_10_2.5	30	232	7	0.068
GP_1.5_10_1.75	30	257	7	0.084
GP_1.5_7.5_1.0	30	257	7	0.084
GP_2.5_5.0_1.75	61	470	11	0.123

The highest surface area obtained for GP_2.5_5.0_1.75 (61 m^2 g^{-1}) is comparable to the result obtained by Li et al. [47], who observed a GP prepared using coal FA collected by an electro-precipitation process from an electric power station in Western Australia as a precursor with a surface area of 56 m^2 g^{-1} [1]. The increase in the surface area of geopolymer is primarily caused by the increase in its porosity compared to FA. When FA dissolves, it releases alumina, silica, iron, and other components into the solution. These monomers react to form oligomers, which then produce geopolymer gel. A higher degree of reaction leads to a denser gel with a compact microstructure and lower porosity. On the other hand, a lower degree of reaction results in a more porous geopolymer characterized by a more open microstructure and higher surface area [48].

3.1.2. Surface chemistry

Fig. 1 represents the results obtained using the FT-IR spectroscopy. Comparing the spectra of the GP and FA samples reveals some differences in the peak intensities and positions.

FT-IR spectroscopy can provide information on the transition of vibrations due to small structural changes. In all the analyzed GP samples, a peak of about 3400 cm^{-1} was observed, indicating the presence of hydroxyl groups (-OH) in the GP matrix [47]. The narrow band at about 1600 cm^{-1} was also observed, suggesting the presence of H—O-H from water hydroxyl groups [49,50]. In the spectra of both FA and GP samples, a peak at approximately 1400 cm^{-1} followed by a weak band at nearly 870 cm^{-1} was observed, indicating the presence of C—O bending vibrations for the CO_3^{2-} group [50]. It is believed that these bands formed due to the carbonation of the surface by atmospheric CO_2 [51].

The band observed at 1037 cm^{-1} in the FA spectrum corresponds to the asymmetric stretching vibrations of Si-O-T (T-tetrahedral Al or Si). In all GP samples, this peak was in a lower wavenumber range of 1000–980 cm^{-1} while increasing in intensity, indicating the successful incorporation of the FA into the GPs matrix [52]. This shift reflects structural changes in the Si-O-Si bonds, attributed to bond breaking and formation during geopolymerization. Specifically, the shift to lower wavenumbers suggests alterations in bond length and angle within the gel network [48]. These modifications enhance the material's chemical reactivity and introduce more active sites (*e.g.*, Si-OH groups), improving the material's ability to interact with and retain contaminants. Also, the altered Si-O-Si bonds might enhance specific interactions, such as hydrogen bonding or van der Waals forces, thereby improving adsorption efficiency [53].

The band at 700 cm^{-1} is not reported in the literature regarding geopolymers and is absent in the analysis of other fly ashes as well. This suggests that this spectral feature may not be characteristic of the investigated materials [54,55]

Furthermore, bands around 580–560 cm^{-1} in the GP samples are attributed to the ring vibrations of Si-O bonds in the silicate network [50]. In a previous study conducted by Syial et al. [48]., FT-IR analysis was performed on GPs prepared from FA to use as adsorbents. The analysis revealed specific bands in the spectrogram that indicate certain molecular groups. In particular, bands around 3400 cm^{-1} and 1600 cm^{-1} were observed, corresponding to the H—O-H and -OH groups. In addition, the presence of Si-O-T bonds (where T represents Al or tetrahedral Si) was indicated by bands at 1058 cm^{-1} for FA and 1004 cm^{-1} for the GP. The reduction in the intensity of this band in the GP spectrum suggests a characteristic change associated with geopolymerization.

XRD analysis was conducted to investigate the various crystal phases in FA and GPs samples (GP_2.0_7.5_1.75, GP_2.0_10_2.5, GP_1.5_10_1.75, GP_1.5_7.5_1.0, and GP_2.5_5.0_1.75). The resulting diffraction diagrams are presented in Fig. 2.

XRD analysis of the FA revealed several crystalline phases, notably quartz, mullite, and calcite (Figure S3), with calcite ($CaCO_3$) being the

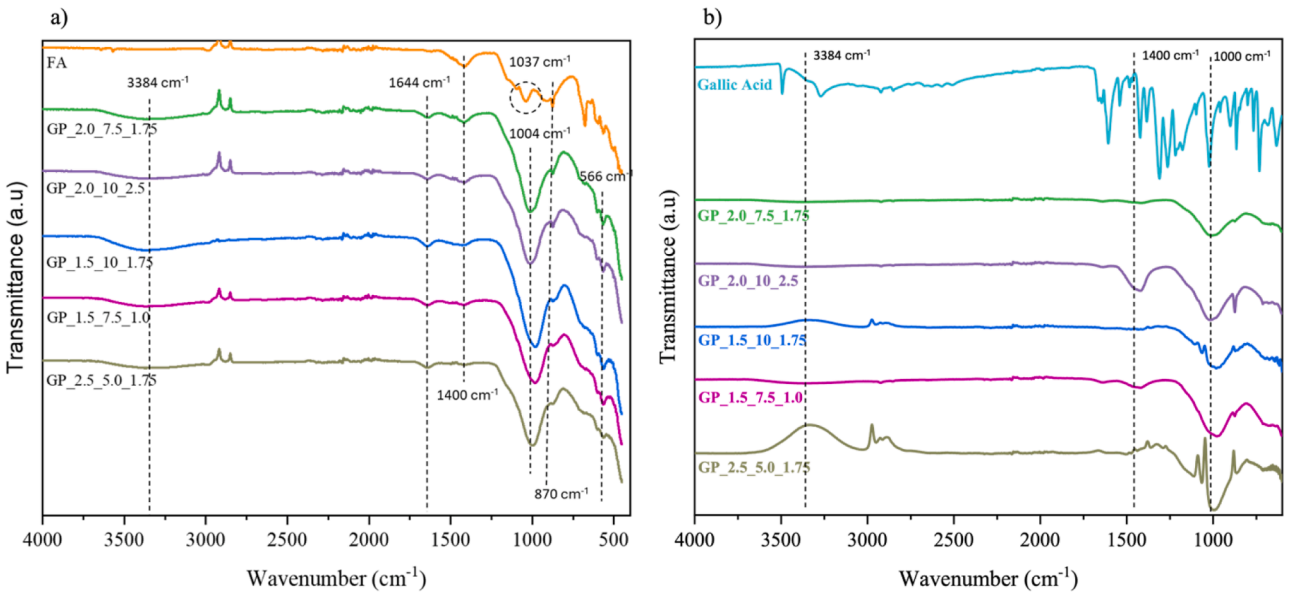

Fig. 1. FT-IR comparison between: a) FA and fresh geopolymers and b) recovered geopolymers from GA adsorption.

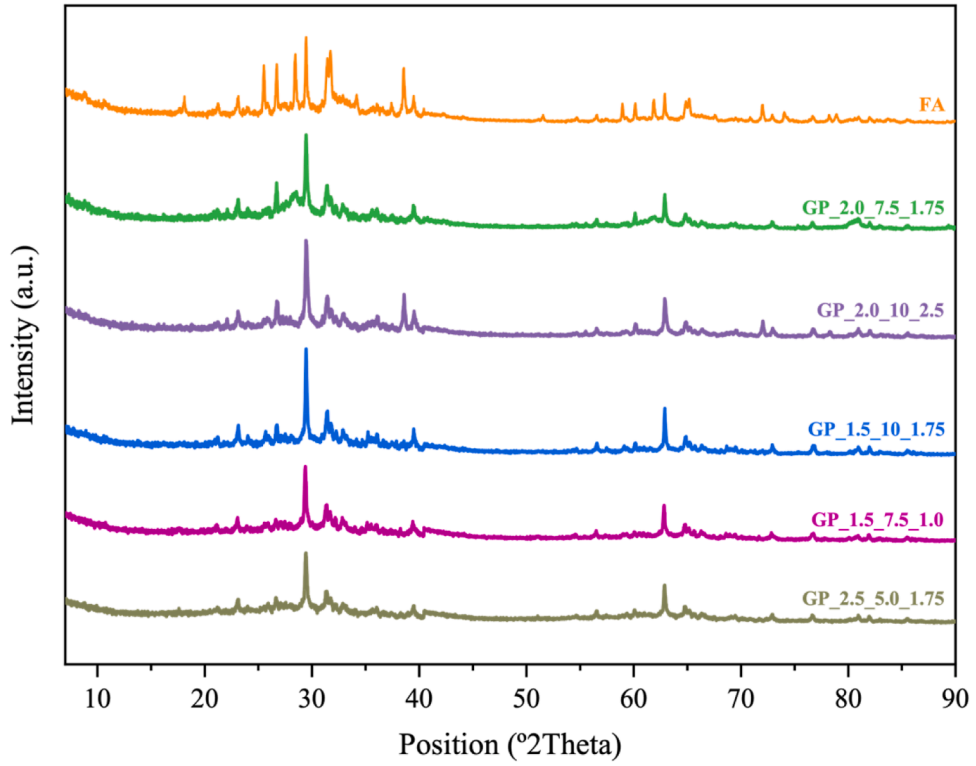

Fig. 2. XRD diffractograms of FA and selected GPs samples.

most prominent. This finding aligns with ICP-OES results (Table S1), indicating that calcium is the most abundant element in FA, resulting from the incineration of calcium-rich materials such as food waste, construction debris, and plastics in MSW [56,57]. XRD analysis indicates that the primary crystalline phases (quartz, mullite, and calcite, Figure S3) in FA are also present in the final geopolymeric products, suggesting the retention of undissolved FA particles in these materials [58,59]. Unreacted fly ash affects the material's porosity and specific surface area, as it has a smaller surface area (13 m^2 g^{-1}) than geopolymers (30 - 60 m^2 g^{-1}) [60]. Also, a complete geopolymerization reaction, combined with the FA negative surface charge and the activators' alkaline conditions, reinforces the GPs' alkalinity, which is known to enhance the adsorption of cationic compounds [61].

Additionally, the XRD analysis of FA shows four distinct peaks in the range of $2\theta = 18°$ to $30°$; in the GPs - XRD patterns, the peak positions are slightly shifted to higher angles ($2\theta = 21° - 35°$). This shift implies that the amorphous phase of FA undergoes a transformation during the synthesis of the GPs, forming a new amorphous phase.

The surface charge of GPs depends on the surrounding environment's pH. The surface may be positively charged, negatively charged, or have no charge at specific pH values. This parameter is considered a significant descriptor of variable-charge surfaces. The results of pH_{PZC},

basicity, and acidity are shown in Table 2.

The *pHPZC* value for all the GPs analyzed was in the range of *ca.* 8. This suggests that the GPs will exhibit a positive charge below this value due to increased hydrogen ion (H^+) concentration. Conversely, when the pH exceeds this value, the GPs will carry a negative charge as hydroxide ions (OH^-) concentration increases. The pH_{PZC} value is an essential parameter for describing variable-charge surfaces, and the consistency of values observed across the analyzed GPs indicates a uniform surface charge behavior [62].

Some FA-derived GP materials exhibited positive surface charges, effectively adsorbing negatively charged pollutants. One example is the GP investigated by Siyal et al. [48] who examined the adsorption behavior of anionic surfactants. Considering this property of geopolymeric materials, it becomes plausible to investigate the adsorption potential of other negatively charged pollutants such as nitrate, nitrite, chloride, sulfide, and fluoride treatment applications.

3.1.3. Morphology

The morphology of the FA and GP samples was studied using SEM/EDS microscopy. The microstructure of FA (Fig. 3a) is intricate and multifaceted, characterized by an amalgamation of independent and agglomerated particles that appear round and spherical but vary in size and shape. These particles are often interspersed with interconnected pores, further complicating the overall structure [63]. The raw FA (Fig. 3a) exhibits spherical pearl-like particles typical of this material, with well-defined and smooth surfaces. The spherical morphology is a characteristic of FA due to its combustion origin. The SEM images of FA serve as a baseline for understanding the transformations during geopolymerization.

Moving along the Si/Al, GP_2.5_5.0_1.75 (Fig. 3b) stands out with a significantly more homogeneous structure than the other GPs. The SEM images of GP_2.5_5.0_1.75 reveal fewer unreacted FA particles and a denser, more cohesive GP matrix. Instead of the formation of spherical units, the surface of GP is covered by a smooth geopolymeric gel. Thus, the reactivity of FA can be determined according to the amount of spherical pearl-like (identified in the SEM image by the red circles) units formed [64]. The higher Si/Al ratio likely contributed to a more complete geopolymerization process, resulting in a material with greater structural uniformity. The smoother and more interconnected gel-like phases [65] in this GP also suggest that this material has larger pores, as confirmed by the textural properties analysis (Table 1).

Focusing on GP_2.0_7.5_1.75 and GP_2.0_10_2.5 (Fig. 3c and d), which share the same Si/Al ratio of 2 in the synthesis procedure, SEM analysis reveals some similarities in structure, such as the presence of both geopolymerized regions and unreacted FA particles. These GPs also demonstrate relatively larger structures than those observed in GP_1.5_10_1.75 and GP_1.5_7.5_1.0 (Fig. 3e and f). The porous texture and the unreacted FA particles suggest that while there is more significant densification compared to lower Si/Al ratios, the materials are still somewhat heterogeneous [66].

In comparison, GP_1.5_10_1.75 and GP_1.5_7.5_1.0 (Fig. 3e and f) display a more pronounced heterogeneous nature with a Si/Al ratio of 1.5 with unreacted precursor material. The SEM images reveal the geopolymerization process has occurred, but a significant portion of the raw FA particles remains visible. Despite the alkaline activation, the FA particles are not fully transformed, resulting in a mixture of geopolymerized and non-geopolymerized regions. This observation suggests that lower Si/Al ratios can lead to incomplete geopolymerization, resulting in a less dense structure. A similar finding was reported in a study using metakaolin as a source of silicon Si and Al [67]. However, no other studies in the literature have confirmed this specific outcome at the same analysis conditions, highlighting its potential uniqueness and significance in geopolymer research.

The EDS analysis (Table S3) indicated a decrease in CaO content and a corresponding increase in both Al_2O_3 and SiO_2 concentrations in the composition of all GPs compared to the FA. This shift in elemental composition suggests a geopolymerization process [20].

Table 2
Values of pH_{PZC}, basicity and acidity for selected GPs.

GP	pH_{PZC}	Basicity (mmol l^{-1})	Acidity (mmol l^{-1})
GP_2.0_7.5_1.75	8.2	1900	770
GP_2.0_10_2.5	8.8	1925	470
GP_1.5_10_1.75	8.7	1970	705
GP_1.5_7.5_1.0	8.6	1945	900
GP_2.5_5.0_1.75	8.2	1860	950

3.2. Gallic acid adsorption

3.2.1. Response surface methodology

As previously indicated, RSM was employed to explore and dissect the interplay between the response and independent variables. Table 3 summarizes the adsorption capacity of GA at equilibrium, and the removal efficiency of each GP produced.

It can be observed that the Si/Al ratio significantly influences the removal efficiency. The highest removal efficiency values (99 %) were obtained with the materials (GP_2.5_5.0_1.75, GP_2.5_10_1.75, GP_2.5_7.5_1.0, and GP_2.5_7.5_2.5) that have the highest Si/Al ratio used in the experimental design (2.5). On the other hand and comparing them to the lowest removal efficiency (97 %) values (GP_1.5_5.0_1.75, GP_1.5_7.5_1.0, and GP_1.5_7.5_2.5), which are associated with the lowest Si/Al ratio of 1.5, we can conclude that a higher Si/Al ratio enhances removal efficiency.

Notably, GP_2.5_5.0_1.75 emerged as the most effective material, exhibiting the most favorable q_e at ± 18.1 mg g^{-1} and E of 99 %. Featuring the highest S_{BET} surface area (61 m^2 g^{-1}), essential in GA adsorption, it provides increased active sites for interaction, highlighting its optimized performance. The *pHpzc* for GP_2.5_5.0_1.75 was measured at 8.2, suggesting that its surface charge favors GA adsorption over a pH range. Additionally, its basicity of 10.5 mmol l^{-1} supports a highly reactive surface, enhancing the affinity for GA molecules. This correlation (Fig. 4) between a high Si/Al ratio, surface basicity, and adsorption capacity illustrates how these properties optimize the material for effective gallic acid removal.

In contrast, GP_1.5_10_1.75 exhibited comparatively lower performance, showing a q_e of 17.1 mg g^{-1} and a E of 97 %. This lower efficiency aligns with its Si/Al ratio of 1.5, which appears less favorable for GA removal. Additionally, GP_1.5_10_1.75 presented distinct physicochemical characteristics, with a *pHpzc* of 8.78, indicating a slightly more basic surface environment, and a high basicity of 15.3 mmol l^{-1}. Despite having a reasonable S_{BET} surface area of 30 m^2 g^{-1}, this combination of properties did not yield the same adsorption capacity or removal efficiency as observed in materials with a Si/Al ratio of 2.5.

Additionally, p-values were calculated to indicate the statistical significance of each factor, allowing for the identification of which variables had a meaningful impact on adsorption efficiency (ANOVA in Table S4) [68]. The statistical analyses were conducted using the modified form of Eq. (3), as presented in Eq. (11) (ANOVA in Table S5), which was adapted for programming within the software.

$$y = b_0 + b_1x_1 + b_2x_2 + b_3x_3 + b_{11}x_1^2 + b_{22}x_2^2 + b_{33}x_3^2 + b_{12}x_1x_2 + b_{13}x_1x_3 + b_{23}x_2x_3 + \varepsilon \quad (11)$$

Where y is the output response, x_1, x_2, and x_3 are the variables that represent the parameters; the intercept term b_0, provides the predicted mean of y when each x is set to zero; b_1, b_2, and b_3 correspond to the linear term coefficients; b_{11}, b_{22}, and b_{33} are the quadratic term coefficients; b_{12}, b_{13}, and b_{23} are the interaction term coefficients; and to represent unexplained variability, an error term ε is added to the model increase the model's predictive ability and statistical significance (ANOVA in Table S4); the resulting equation is Eq. (12).

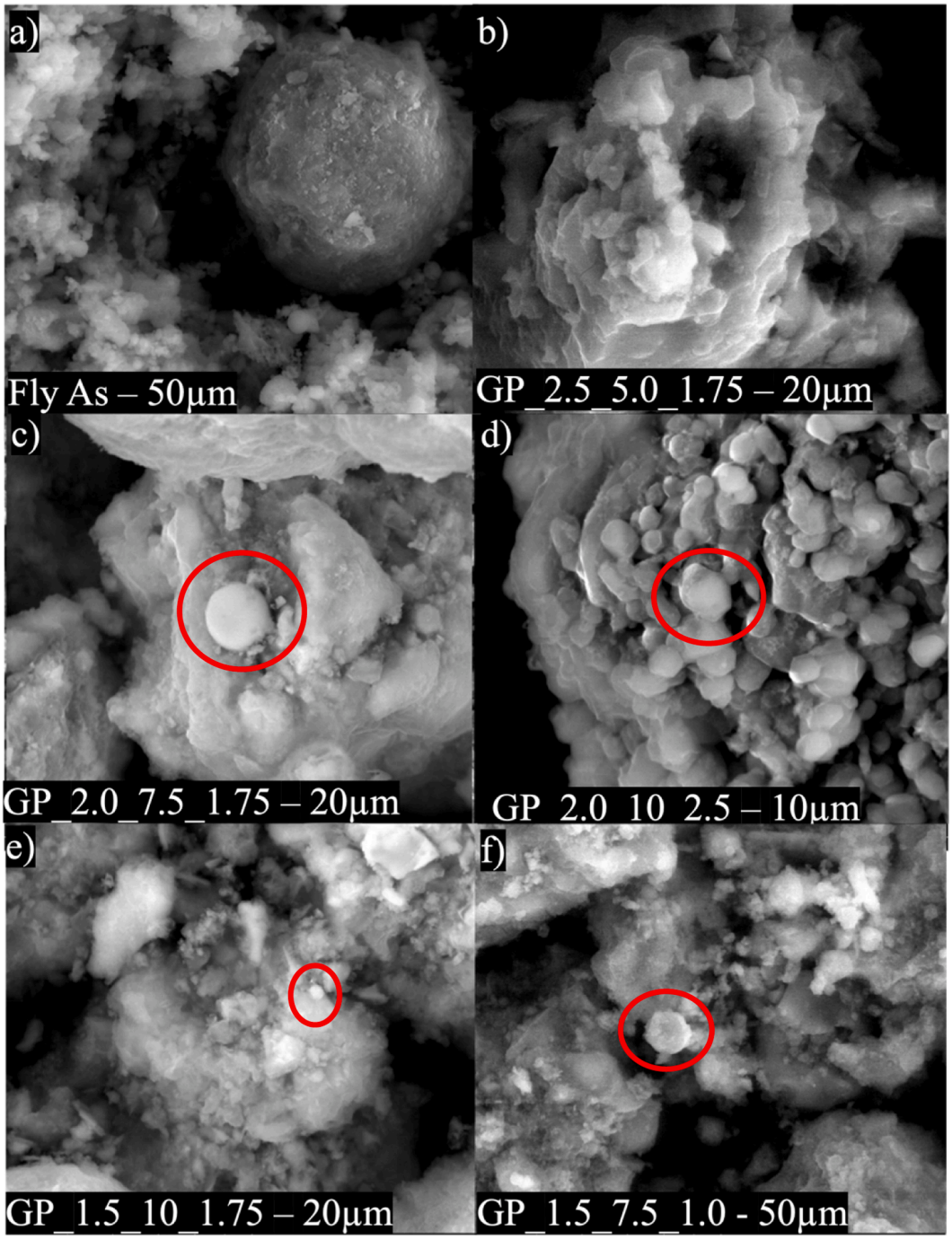

Fig. 3. SEM micrographs of: a) FA, b) GP_2.5_5.0_1.75, c) GP_2.0_7.5_1.75, d) GP_2.0_10_2.5, e) GP_1.5_10_1.75, and f)GP_1.5_7.5_1.0.

$$y = b_0 + b_1x_1 + \ b_2x_2 + b_3x_3 + b_{22}x_2^2 + b_{33}x_3^2 + b_{23}x_2x_3 + \varepsilon \quad (12)$$

Using the equation structured in this form, the results obtained from the statistical analysis are presented in Table 4.

The model's fitted values produced an adjusted R^2 value of 0.800. However, this value is still considered unsatisfactory, suggesting that some experimental data does not align well with the model used. This disparity indicates a discrepancy between the predicted values of the model and the actual experimental results. On the other hand, the *p*-value of the regression is 0.002 and it was considered satisfactory, indicating that at least one of the predictor variables in the model presents a significant relationship with the response variable. Consequently, the regression model demonstrates statistical significance in explaining the variability observed in the response variable.

The estimated coefficient for each factor means the magnitude of the impact on the final response resulting from variations in the respective variables. For example, a coefficient value of 0.97 for variable x_1 indicates that, on average, a one-unit increase in x_1 is associated with an average 0.97 unit increase in the response variable, assuming all other variables stay unchanged. Based on the provided coefficients, it is evident that the variable with the most significant influence on the response is x_1, representing the Si/Al ratio. This conclusion is supported by its Prob>|t|, which is below the threshold of 0.05 commonly used to determine statistical significance. Specifically, as indicated in Table 4 and Table S4, the Prob>|t| value for x_1 is 0.001, reflecting a strong significance level. In contrast, the Prob>|t| values for x_2 and x_3 are 0.8 and 0.4, respectively, suggesting that these factors have a lower

Table 3
Adsorption capacity (q_e) and removal efficiency (E) of GA results.

Sample	q_e (mg g^{-1})	Response y_1 E (%)
GP_1.5_5.0_1.75	17.8	97
GP_2.5_5.0_1.75	18.1	99
GP_1.5_10_1.75	17.1	97
GP_2.5_10_1.75	17.3	99
GP_1.5_7.5_1.0	17.2	98
GP_2.5_7.5_1.0	17.7	99
GP_1.5_7.5_2.5	17.2	97
GP_2.5_7.5_2.5	17.2	99
GP_2.0_5_1.0	18.2	98
GP_2.0_10_1.0	17.8	98
GP_2.0_5.0_2.5	17.4	98
GP_2.0_10_2.5	17.5	98
GP_2.0_7.5_1.75	17.6	98
GP_2.0_7.5_1.75	17.5	97
GP_2.0_7.5_1.75	17.6	98

statistically significant impact under the same criteria. Additionally, the squared term of x_3, denoting Na_2SiO_3/NaOH, significantly impacts the responses. This indicates that nonlinear effects related to this factor play a crucial role in the adsorption efficiency.

The observations regarding the t-values and *p*-values further confirm the influence of the factors on the responses. A higher t-value corresponds to a lower p-value; for a term to be considered statistically significant, the *p*-value should be less than 0.05. By evaluating the *p*-values for each factor, it can be reaffirmed that both x_1 (Si/Al ratio) and x_3^2 (Na_2SiO_3/NaOH) significantly affect the GPs efficiency of GA removal.

To better understand this factor, for each contour plot, one factor was maintained constant at its midpoint value ($x_i = 0$). In contrast, the other two factors varied from their minimum to maximum range. This approach explains how changes in the independent variables affect the response variable by examining the contours of the response levels at different combinations of the variable factors.

In Fig. 5a, where the Na_2SiO_3/NaOH (1.75) factor is held constant while varying the other two factors, the removal efficiency increases with a higher Si/Al ratio, as expected. The curved nature of the lines further indicates a nonlinear relationship between the molar concentration of NaOH and the Si/Al ratio.

In Fig. 5b, with the x_2 (NaOH of 7.5 M) factor held constant and the other factors varied, a similar trend is observed: the percentage of removal increases as the Si/Al ratio rises. Notably, there is no clear linear relationship between the Si/Al ratio (x_1) and the Na_2SiO_3/NaOH ratio (x_3), suggesting that their interaction is more complex and does not conform to a simple linear trend.

Fig. 5c shows that when the Si/Al ratio is fixed, an increase in the Na_2SiO_3/NaOH ratio initially results in decreased removal efficiency. However, once the Na_2SiO_3/NaOH ratio approaches approximately 2, further increases in this ratio lead to enhanced removal efficiency. Overall, it appears that increasing the NaOH concentration tends to decrease removal efficiency when paired with Na_2SiO_3/NaOH ratios below 2. Conversely, for ratios exceeding 2, an increase in NaOH concentration enhances removal efficiency.

It is important to note that analyzing only the removal efficiency is not sufficient to evaluate the performance of an adsorbent, as it only considers the initial and final concentration of the adsorbate in the fluid phase, neglecting other factors involved in adsorption, such as the mass of the adsorbent used and the volume of the solution. Additionally, it does not consider other properties of the adsorbents.

3.2.2. *Equilibrium isotherms*

The equilibrium isotherms were studied by fitting Langmuir and Freundlich's models described by Eqs. (6) and (7), respectively, to the five selected GPs. Table 5 shows the parameters obtained by the equilibrium fits for the chosen materials GP_2.0_7.5_1.75, GP_2.0_10_2.5, GP_1.5_10_1.75, GP_1.5_7.5_1.0, and GP_2.5_5.0_1.75.

Analyzing the values of r^2 obtained in the fitness of each of the models for the GPs, it can be observed that both models adequately described the experimental equilibrium data. However,

Table 4
The influence of model coefficients linking response to a variable.

Term	Coefficient	Estimation	Std. Error	t value	Prob>|t|
Intercept	b_0	98.062	0.187	523.708	2.2E-16
x_1	b_1	0.974	0.159	7.066	1.06E-01
x_2	b_2	−0.037	0.159	−0.272	0.792
x_3	b_3	−0.139	0.159	−1.007	0.343
x_2:x_3	b_{23}	0.130	0.225	0.667	0.523
x_2^2	b_{22}	0.126	0.234	0.623	0.551
x_3^2	b_{33}	0.538	0.234	2.66	0.029
R^2	**Adj. R^2**	***p*-value**			
0.880	0.800	0.002			

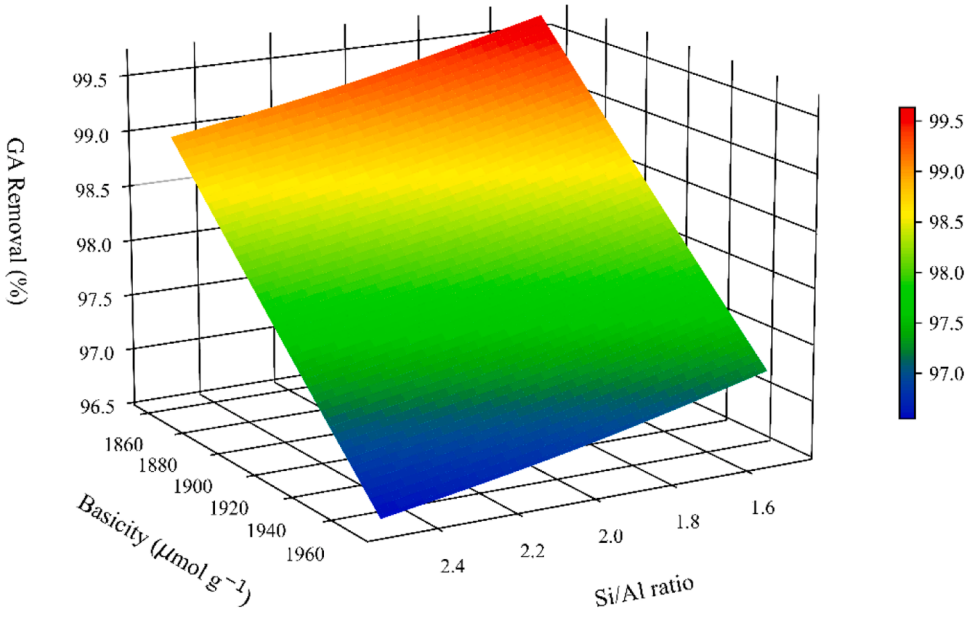

Fig. 4. Correlation between Si/Al ratio, surface basicity, and adsorption capacity.

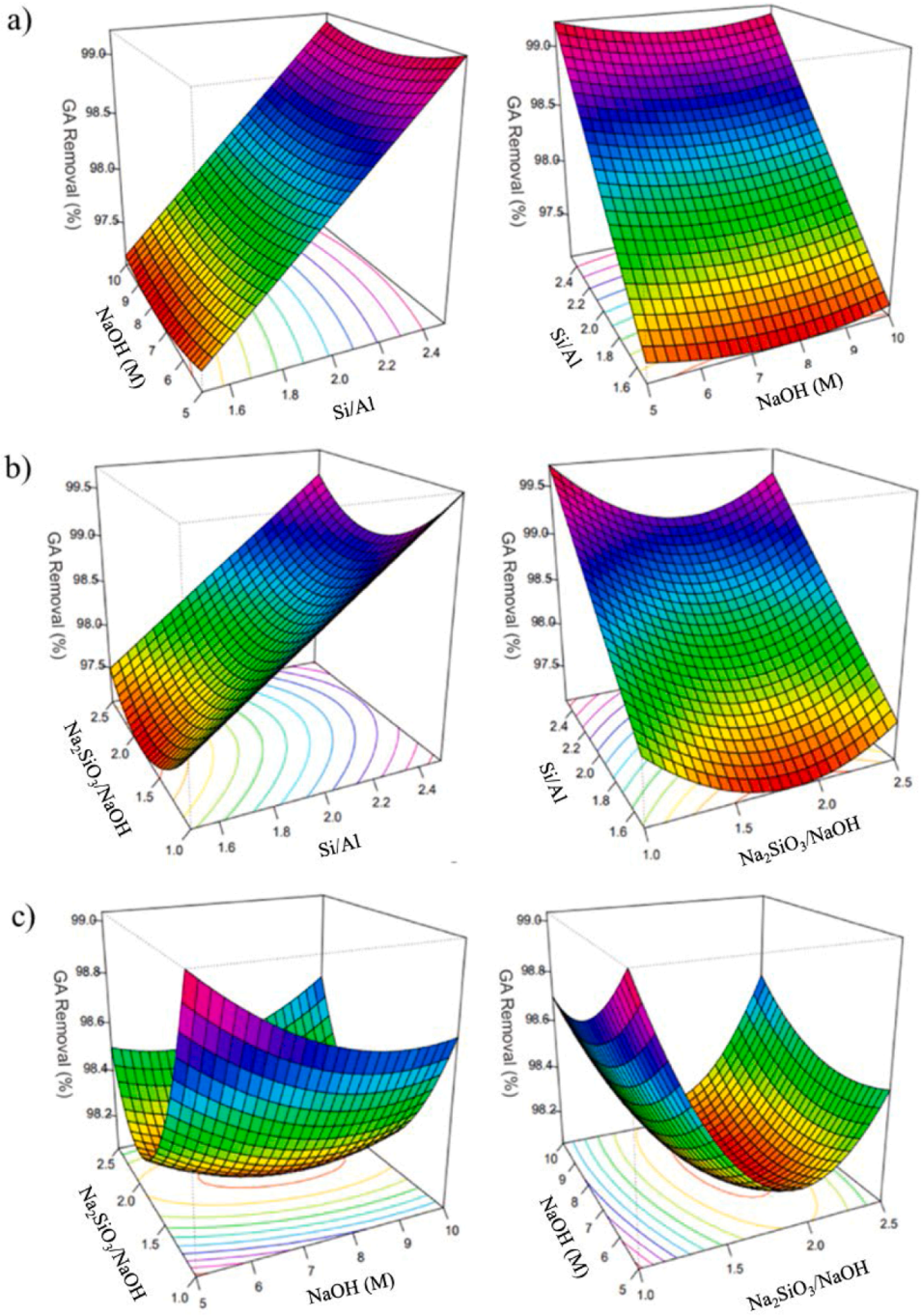

Fig. 5. 3D Contour graphs of (GA = 50 mg l^{-1}, GPs = 2.5 g l^{-1}, T = 50 °C, agitation = 300 rpm, and time = 480 min) showing removal efficiency (E %) as a function of: a) NaOH (x_2) and Si/Al (x_1); b) Na_2SiO_3/NaOH (x_3) and Si/Al (x_1), and c) Na_2SiO_3/NaOH (x_3) and NaOH (x_2).

Table 5
Parameters of equilibrium models.

GP	Langmuir			Freundlich		
	q_m (mg g^{-1})	K_L (L mg^{-1})	r^2	K_F (L g^{-1})	n_F	r^2
GP_2.0_7.5_1.75	39.2	0.4	0.98	11.4	2.1	0.98
GP_2.0_10_2.5	75.8	0.4	0.98	22.0	1.4	0.97
GP_1.5_10_1.75	58.2	0.2	0.98	10.6	1.6	0.98
GP_1.5_7.5_1.0	41.6	0.7	0.95	15.7	1.9	0.95
GP_2.5_5.0_1.75	40.8	1.8	0.95	22.0	2.3	0.96

GP_2.0_7.5_1.75, GP_1.5_10_1.75 and GP_1.5_7.5_1.0 all achieved the same r^2 value for both models Table 6.

For GP_2.0_10_2.5, which obtained a better fit to the Langmuir model and the highest q_m of 75.8 mg g^{-1}, other studies have also reported similar results for GPs produced from the FA in adsorption. Hijazi et al. [39], who investigated the use of GPs for phenol removal, another phenolic compound, reported an uptake capacity of 166 mg g^{-1}, described by the Langmuir model, indicating a monolayer adsorption mechanism. On the other hand, Liu et al. [69] reported a better fit in their equilibrium data on Pb removal with the Langmuir model.

Freundlich model fit well with the adsorption results obtained with the GP_2.5_5.0_1.75 sample. This optimal fit suggests that adsorption occurs on solids with heterogeneous surfaces, where the active sites

Table 6
R_L calculated values.

C_0 (mg l^{-1})	R_L				
	Geopolymer Sample				
	GP_2.0_7.5_1.75	GP_2.0_10_2.5	GP_1.5_10_1.75	GP_1.5_7.5_1.0	GP_2.5_5.0_1.75
100	0.02	0.02	0.04	0.01	0.01
75	0.03	0.03	0.06	0.02	0.01
50	0.05	0.04	0.09	0.02	0.01
30	0.07	0.07	0.13	0.04	0.02
10	0.19	0.18	0.32	0.11	0.05

possess varying affinities and energies for adsorption. Sites with the highest affinity for the adsorbed molecules will be preferentially occupied [70]. Our results can be compared to previous research that utilized FA to produce GP-based adsorbents. Tian and Sasaki [71] found a better fit for the Freundlich model when they studied the adsorption of arsenate (AsO_4^{3-}). And also, Qiu et al. [72] reported a better fit of the Freundlich model in removing Cr(VI).

The best fit of the isotherms to the Freundlich model proposes that adsorption occurs on solids with heterogeneous surfaces, where the active sites have varying affinities and adsorption energies. Sites with the highest affinity for the adsorbed molecules will be preferentially occupied [70]. This results in a decrease in the binding energy of the remaining sites, following an exponential decay profile. Then, the multilayer arrangement is formed during adsorption [73]. However, it is impossible to state that GPs exhibit this behavior during adsorption since the Langmuir model also fits the experimental data well, and further studies are needed to draw more profound conclusions.

By further analyzing the obtained n_F values from fitting the Freundlich model, it is evident that all the values fall within the expected range of 1 to 10, indicating favorable conditions for adsorption. Furthermore, by examining the calculated R_L, all values are between 0 and 1. This indicates a meaningful affinity of the adsorbate for the adsorbent, which suggests good adsorption processes for all the GPs analyzed

Fig. 6 displays the plots describing the fits of the two equilibrium models. These graphs visually represent how the models fit with the experimental data.

The results of the Langmuir fit show that the highest adsorption capacities were obtained by GP_2.0_10_2.5 and GP_1.5_10_1.75, with values of 75.8 mg g^{-1} and 58.1 mg g^{-1}, respectively. The other GPs exhibited similar adsorption capacities around 40 mg g^{-1}. Notably, the GPs with a higher molar concentration of NaOH (10 M) showed the highest adsorption capacities. Additionally, GP_2.0_10_2.5 stands out as the only GP with the maximum ratio of Na_2SiO_3/NaOH in its formulation, which may have also contributed to its superior adsorptive capacity.

Moreover, the recovered GPs after adsorption were reanalyzed using FTIR spectroscopy to investigate potential chemical changes induced by the adsorption process; the spectra are presented in Fig. 1b.

The region at 3384 cm^{-1}, associated with -OH groups, reveals key insights into the interaction between geopolymers and GA during adsorption. A decrease in intensity suggests that -OH groups on the GP_2.0_7.5_1.75, GP_2.0_1.0_2.5, and GP_1.5_7.5_1.0 surface are consumed through hydrogen bonding with GA, indicating a chemical adsorption mechanism. In contrast, increased intensity observed in GP_2.5_5.0_1.75 spectra may result from the retention of water molecules on the surface or the generation of new -OH groups after adsorption [39]. This behavior could arise from activating additional surface sites or chemical changes, such as GA reactions.

The region at 1000 cm^{-1}, corresponding to Si-O-Si or Si-O-Al bonds, displays variations in intensity or peak shifts, which indicate surface adsorption in the geopolymer matrix. These changes may be attributed to direct chemical interactions between GA and the Si-O-Si or Si-O-Al network, leading to new bonds.

New peaks, particularly in regions associated with C═C and C—H vibrations at 1400 cm^{-1}, may appear after adsorption. These additional signals provide evidence for the presence of GA adsorbed on the surface of the geopolymers, further confirming the occurrence of adsorption processes.

Finally, in the findings on adsorption equilibrium, was noticed that the q_m values showed a direct correlation with the increase in pH_{pzc} in the geopolymers. Materials with higher q_m values, such as GP_2.0_10_2.5 (75.8 mg g^{-1}), GP_1.5_10_1.7 (58.2 mg g^{-1}), GP_1.5_7.5_1.0 (41.6 mg g^{-1}), GP_2.5_5.0_1.75 (40.8 mg g^{-1}), and GP_2.0_7.5_1.75 (39.2 mg g^{-1}), exhibited pH_{pzc} values of 8.8, 8.7, 8.6, 8.2, and 8.2, respectively. This trend suggests that the increase in pH_{pzc} led to a corresponding rise in the q_m, as represented by the Langmuir model. The pHpzc, which indicates the point where the surface charge of the material is neutral, likely influences the electrostatic interactions between the geopolymers and adsorbates. As the pHpzc increases, the material becomes more favorable for adsorption, particularly ionic species. This is consistent with the Langmuir model's assumption of monolayer adsorption on a surface with a fixed number of identical sites.

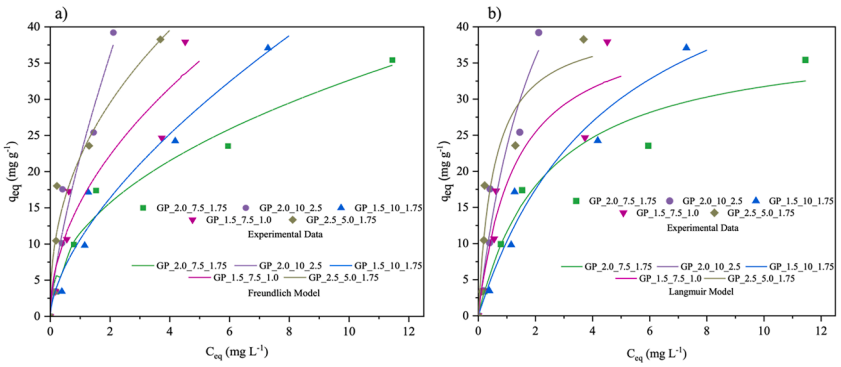

Fig. 6. Adsorption isotherms using (a) Freundlich and (b) Langmuir models for experimental data obtained with GP_2.0_7.5_1.75, GP_2.0_10_2.5, GP_1.5_10_1.75, GP_1.5_7.5_1.0, and GP_2.5_5.0_1.75 adsorbents.

3.2.3. Kinetic modelling

The kinetic models represented by Eqs. (8), (9), and (10) were fitted to experimental adsorption kinetics data. Table 7 presents the kinetic fitting data obtained for the adsorption of GA onto the 15 different GP samples.

Observing the value of r^2, the obtained results indicate that, in general, the pseudo-first-order model fits better with experimental data. Additionally, the calculated adsorptive capacity in the equilibrium (q_e) for these GPs and this model was closer to the experimental data (q_{exp}), validating its applicability in the description of GA adsorption kinetics data.

Interestingly, all the chosen materials GP_2.0_7.5_1.75, GP_2.0_10_2.5, GP_1.5_10_1.75, GP_1.5_7.5_1.0, and GP_2.5_5.0_1.75 exhibited r^2 values of 0.99 for both the pseudo-first-order and pseudo-second-order models, indicating a good fit for the two models. However, all GPs exhibited an r^2 value that was slightly higher (for the pseudo-second-order model) or equally in both models and the experimental adsorptive capacity (q_{exp}) value closest to the value calculated (q_e).

Analyzing the best-fitting model, which proved to be more concise for all geopolymers—the pseudo-first-order model, and among the characterized GPS, GP_2.5_5.0_1.75, which exhibited the highest BET surface area (61 $m^2\ g^{-1}$), also achieved the highest experimental adsorption capacity (q_{exp}) of 18.1 mg g^{-1}. Similarly, GP_2.0_5.0_1.0 demonstrated both q_{exp} and q_e values of 18.3 mg g^{-1}. These materials share similar formulations, differing only in their Na_2SiO_3/NaOH ratio.

In contrast, the other characterized GPs (GP_2.0_10_2.5, GP_1.5_10_1.75, and GP_1.5_7.5_1.0) exhibited q_{exp} and q_e values ranging from 17.2 to 17.5 mg g^{-1}, which were comparable among them. These materials also displayed similar BET surface areas, ranging between 30 $m^2\ g^{-1}$.

However, GP_2.0_7.5_1.75, which achieved an r^2 of 0.99 for both models, demonstrated a q_e of 20 mg g^{-1} in the pseudo-second-order model. This material had a BET surface area of 35 $m^2\ g^{-1}$, highlighting its potential for adsorption applications.

In a comprehensive review of GP application for heavy metal and dye removal, Liang K.et al. [74] summarized several studies focused on the removal of cationic dyes, which are particularly effective due to their negative surface charge and the alkaline conditions created by the activators. For instance, Acisli et al. [75] efficiently removed Basic Yellow 2, while Zhang et al. [76] and Wattanasiriwech et al. [77] successfully removed Methylene Blue using FA-based geopolymers and foam mortar, respectively. These materials demonstrate strong electrostatic interactions that facilitate cationic dye adsorption, as the negatively charged geopolymer surfaces attract the positively charged dye molecules, enhancing the adsorption process. Our materials also exhibited adsorption through electrostatic interactions, characteristic of cationic GPs. The pH_{PZC} values of our geopolymers ranged from 8.2 to 8.8, indicating that the surface charge of the materials is negative at neutral and basic pH. The basicity values, varying between 15.3 and 9.8, further reinforce the alkalinity of the materials, which is known to enhance the adsorption of cationic compounds.

As for the GPs that also showed good fits with the pseudo-second-order model, similar results have been reported in the literature utilizing GPs derived from FA. Purbasari et al. [78]. observed that the pseudo-second-order model provided the best fit for the removal of Cu (II) and Fe(II) using geopolymers. Similarly, Liu et al. [69] the same model provided the best fit for Pb removal, and Zhang and Liu [79] studied dye adsorption and obtained a better fit with the pseudo-second-order model. Furthermore, for heavy metal removal, the review made by Liang K.et al. [74] concluded that the adsorption behavior of these materials typically involves a combination of physical and chemical adsorption processes occurring simultaneously.

This study investigated the adsorption rate regarding possible limiting steps of liquid film diffusion, intraparticle diffusion, or both. Analysis of the intraparticle diffusion model fit revealed that the r^2 values were all below 0.98 for the GPs examined, and the intercept (I) was not equal to zero, suggesting that intraparticle diffusion was probably not the only rate-limiting step. Hence, it can be inferred that the kinetics of the adsorption process were probably controlled by both the liquid film and intraparticle diffusion [80].

Additionally, Fig. 7 illustrate the graph describing the best fit pseudo-first-order model relative to the experimental data evaluated for GP_2.0_7.5_1.75, GP_2.0_10_2.5, GP_1.5_10_1.75, GP_1.5_7.5_1.0, and GP_2.5_5.0_1.75.

For all materials, during the initial stages of adsorption, there is an increase in the amount of GA retained per unit mass of adsorbent. This occurs because, during this period, active sites have greater availability, favoring higher adsorption rates [25]. As time passes, the number of active sites available to adsorb the GA decreases, and the already adsorbed pollutant molecules prevent the entry of new molecules. As a result, the kinetics slows until equilibrium is reached, where no significant variations in adsorption capacity are observed over time [74].

During the initial minutes of the adsorption process, there is a rapid and significant increase in adsorbate retention, followed by equilibrium at approximately 200 min. GP_2.0_7.5_1.75 presents a slightly different behavior; the increase in the response variable is not as fast at the beginning compared with the other GPs, and its equilibrium is reached around 300 min. Moreover, it is noticeable that GP_2.0_10_2.5, GP_1.5_10_1.75, GP_1.5_7.5_1.0, and GP_2.5_5.0_1.75 exhibit similar behavior.

Table 7
Parameters of kinetic models for pseudo-first and pseudo-second order and intraparticle diffusion.

GP	q_{exp} (mg g^{-1})	Pseudo-first order			Pseudo-second order			Intraparticle diffusion		
		q_e (mg g^{-1})	k_1 (min^{-1})	r^2	q_e (mg g^{-1})	k_2 (g $mg^{-1}min^{-1}$)	r^2	I (mg g^{-1})	k_{id} (mg $g^{-1}min^{-0.5}$)	r^2
GP_2.0_7.5_1.75	17.1	17.1	0.01	0.99	20.9	0.001	0.99	0.12	0.8	0.97
GP_2.0_7.5_1.75	17.4	17.5	0.02	0.99	19.4	0.002	0.97	0.67	0.9	0.89
GP_2.5_7.5_2.5	17.3	17.3	0.12	0.99	17.5	0.025	0.99	1.58	1.0	0.73
GP_2.0_5.0_2.5	17.5	17.2	0.20	0.99	17.5	0.047	0.99	1.61	1.0	0.72
GP_2.0_5_1.0	18.3	18.3	0.03	0.99	19.8	0.003	0.98	0.94	1.0	0.86
GP_2.0_10_2.5	17.5	17.5	0.18	0.99	17.7	0.056	0.99	1.67	1.0	0.71
GP_1.5_7.5_2.5	17.3	17.2	0.08	0.99	17.8	0.010	0.99	1.39	1.0	0.77
GP_1.5_5.0_1.75	17.3	17.5	0.03	0.97	19.1	0.002	0.95	0.80	0.9	0.86
GP_2.5_7.5_1.0	17.8	17.7	0.38	0.99	17.7	1.241	0.99	1.75	1.0	0.70
GP_1.5_10_1.75	17.2	16.9	0.23	0.99	17.2	0.078	0.99	1.61	0.9	0.72
GP_1.5_7.5_1.0	17.3	17.3	0.23	0.99	17.3	0.129	0.99	1.68	1.0	0.71
GP_2.5_10_1.75	17.4	17.4	0.03	0.98	18.9	0.003	0.95	0.91	0.9	0.85
GP_2.5_5.0_1.75	18.1	17.7	0.15	0.99	18.1	0.028	0.99	1.62	1.0	0.73
GP_2.0_7.5_1.75	17.7	17.5	0.08	0.99	18.2	0.010	0.99	1.40	1.0	0.77
GP_2.0_10_1.0	17.8	17.9	0.05	0.98	18.9	0.005	0.96	1.25	1.0	0.79

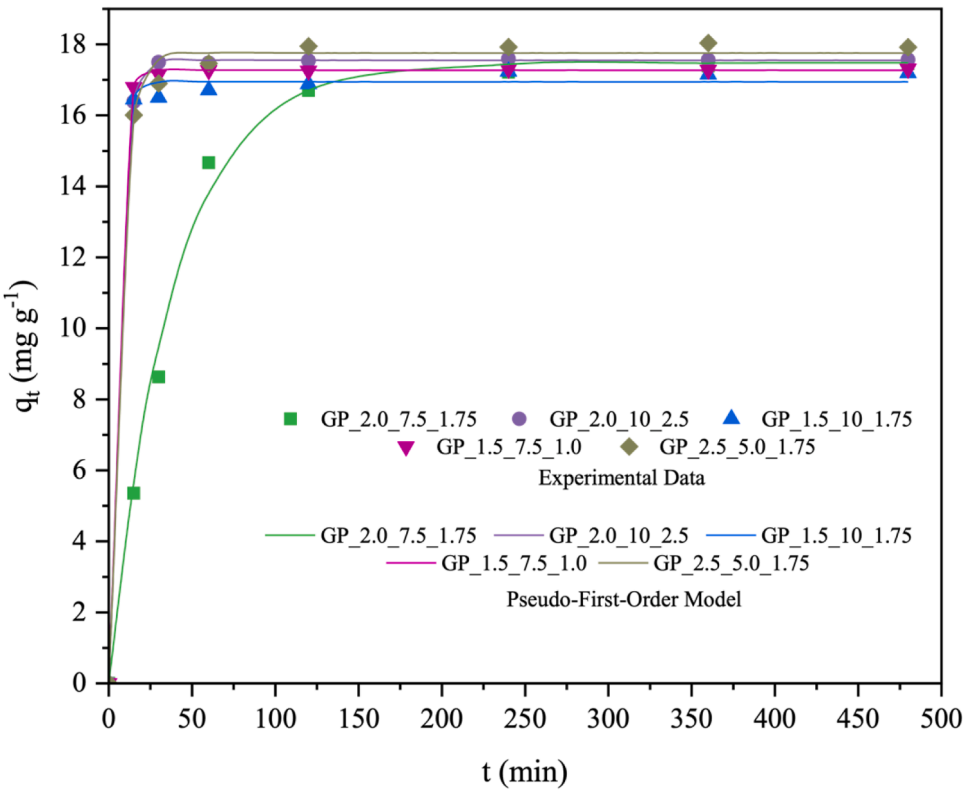

Fig. 7. Fitting the kinetic models to the experimental data for GP_2.0_7.5_1.75, GP_2.0_10_2.5, GP_1.5_10_1.75, GP_1.5_7.5_1.0, and GP_2.5_5.0_1.75.

4. Conclusions

All produced geopolymers effectively removed the target pollutant, and the Box-Behnken design revealed that the Si/Al mass ratio significantly influenced GA removal. Characterization of FA through ICP-OES confirmed its suitability for geopolymer synthesis due to its high calcium, silica, and aluminum content. Improvements in porosity and surface area were noted in the GPs, with GP_2.5_5.0_1.75 achieving a surface area of 61 m^2 g^{-1}. FT-IR analysis confirmed successful geopolymerization, while SEM and XRD analyses showed structural differences and predominance of calcite. The GPs exhibited a basic nature with pH_{PZC} values around 8, enhancing their electrostatic attraction to GA during adsorption. Kinetic studies indicated a good fit to the pseudo-first-order model, achieving equilibrium in approximately 200 min. The GPs generally followed the Freundlich model, indicating favorable adsorption conditions, particularly for GP_2.0_10_2.5, which exhibited the highest maximum adsorption capacity of 75.9 mg g^{-1}. Overall, this research demonstrates the potential of producing geopolymers optimized for adsorption through a systematic experimental approach (DOE). Geopolymers offer several advantages over traditional adsorbents, including lower production temperatures and pressures, reduced energy consumption, and the use of industrial by-products like fly ash, making the process more sustainable. These materials have the potential for application in catalysis, heavy metal removal, and civil engineering applications. By optimizing various formulations, this work provides a strong foundation for scaling up geopolymers into permeable barriers for tertiary treatment, contributing to large-scale environmental remediation.

Funding

This work was supported by national funds supported this work through FCT/MCTES (PIDDAC): CIMO, UIDB/00,690/2020 (DOI: 10.54499/UIDB/00,690/2020) and UIDP/00,690/2020 (DOI: 10.54499/UIDP/00,690/2020); and SusTEC, LA/P/0007/2020 (DOI: 10.54499/LA/P/0007/2020). We would also like to thank the scientific collaboration under Base-UIDB/50,020/2020, CQVR (UIDB/00,616/2020). The authors are grateful to Sociedade Ponto Verde for the financial support through the project "Avaliação de Ciclo de Vida de materiais geopoliméricos obtidos a partir da valorização de resíduos sólidos urbanos". Ana Paula Silva is supported by the doctoral Grant PRT/BD/153,090/2021 financed by FCT and with funds from NORTE2020, under MIT Portugal Program. Jose L. Diaz De Tuesta acknowledges the financial support through the program of *Atracción al Talento* of *Comunidad de Madrid* (Spain) for the individual research grant and project with reference 2022-T1/AMB-23,946.

Statement

While preparing this work, the authors used ChatGPT to reduce the manuscript size and improve readability. After using this tool, the authors reviewed and edited the content as needed and took full responsibility for the publication's content.

CRediT authorship contribution statement

Ana Paula Ferreira: Writing – original draft, Visualization, Validation, Software, Methodology, Investigation, Formal analysis, Data curation, Conceptualization. **Ana Paula S. Natal:** Writing – original draft, Methodology, Investigation, Formal analysis. **Arthur P. Baldo:** Writing – original draft. **Adriano S. Silva:** Writing – review & editing, Writing – original draft. **Jose L. Diaz de Tuesta:** Writing – review & editing, Writing – original draft, Visualization, Validation, Supervision, Funding acquisition, Conceptualization. **Pricila Marin:** Supervision. **José A. Peres:** Writing – review & editing, Visualization, Supervision, Funding acquisition, Conceptualization. **Helder T. Gomes:** Writing – review & editing, Visualization, Supervision, Project administration, Funding acquisition, Conceptualization.

Declaration of competing interest

The authors declare that they have no known competing financial interests or personal relationships that could have appeared to influence the work reported in this paper. The author is an Editorial Board Member/Editor-in-Chief/Associate Editor/Guest Editor for *[Journal name]* and was not involved in the editorial review or the decision to publish this article.

Acknowledgments

This work was supported by national funds supported this work through FCT/MCTES (PIDDAC): CIMO, UIDB/00690/2020 (DOI: 10.54499/UIDB/00690/2020) and UIDP/00690/2020 (DOI: 10.54499/UIDP/00690/2020); and SusTEC, LA/P/0007/2020 (DOI: 10.54499/LA/P/0007/2020). We would also like to thank the scientific collaboration under Base-UIDB/50020/2020, CQVR (UIDB/00616/2020). The authors are grateful to Sociedade Ponto Verde for the financial support through the project "Avaliação de Ciclo de Vida de materiais geopoliméricos obtidos a partir da valorização de resíduos sólidos urbanos". Ana Paula Silva is supported by the doctoral Grant PRT/BD/153090/2021 financed by FCT and with funds from NORTE2020, under MIT Portugal Program. Jose L. Diaz De Tuesta acknowledges the financial support through the program of Atracción al Talento of Comunidad de Madrid (Spain) for the individual research grant and project with reference 2022-T1/AMB-23946.

Supplementary materials

Supplementary material associated with this article can be found, in the online version, at doi:10.1016/j.ceja.2024.100703.

Data availability

Supporting Data is available in the Supplementary Material.

References

[1] L. Chand Malav, K.K. Yadav, N. Gupta, S. Kumar, G.K. Sharma, S. Krishnan, et al., A review on municipal solid waste as a renewable source for waste-to-energy project in India: current practices, challenges, and future opportunities, J. Clean Prod. 277 (2020) 123227, https://doi.org/10.1016/J.JCLEPRO.2020.123227.
[2] Q. Song, J. Li, X. Zeng, Minimizing the increasing solid waste through zero waste strategy, J. Clean. Prod. 104 (2015) 199–210, https://doi.org/10.1016/J.JCLEPRO.2014.08.027.
[3] EUROPEAN COMMISSION. A new Circular Economy Action Plan For a cleaner and more competitive Europe. Brussels: 2020.
[4] R.M. Novais, G. Ascensão, M.P. Seabra, J.A. Labrincha, Waste glass from end-of-life fluorescent lamps as raw material in geopolymers, Waste Manage. (Oxford) 52 (2016) 245–255, https://doi.org/10.1016/J.WASMAN.2016.04.003.
[5] S.M. Abramov, J. He, D. Wimmer, E.M. Muehe, T. Helle, H. Thorwarth, et al., Thiourea leaching of gold from processed municipal solid waste incineration residues, J. Mater Cycles Waste Manag. 24 (2022) 2243–2254, https://doi.org/10.1007/s10163-022-01476-9.
[6] M. Śliz, K. Czerwińska, A. Magdziarz, L. Lombardi, M. Wilk, Hydrothermal carbonization of the wet fraction from mixed municipal solid waste: a fuel and structural analysis of hydrochars, Energies (Basel) 15 (2022) 6708, https://doi.org/10.3390/en15186708.
[7] D. Chen, L. Yin, H. Wang, P. He, Pyrolysis technologies for municipal solid waste: a review, Waste Manage. (Oxford) 34 (2014) 2466–2486, https://doi.org/10.1016/j.wasman.2014.08.004.
[8] S. Harisankar, R. Vinu, Comprehensive evaluation of municipal solid wastes and mixed feedstocks for commercial hydrothermal liquefaction in bio-refineries, Fuel 339 (2023) 127236, https://doi.org/10.1016/j.fuel.2022.127236.
[9] B. Ren, Y. Zhao, H. Bai, S. Kang, T. Zhang, S. Song, Eco-friendly geopolymer prepared from solid wastes: a critical review, Chemosphere 267 (2021) 128900, https://doi.org/10.1016/J.CHEMOSPHERE.2020.128900.
[10] J. Davidovits, Geopolymers: ceramic-like inorganic polymers, J. Ceramic Sci. Technol. 8 (2017) 335–350, https://doi.org/10.4416/JCST2017-00038.
[11] J. Liu, Y. Xu, W. Zhang, J. Ye, R. Wang, Solidification performance and mechanism of typical radioactive nuclear waste by geopolymers and geopolymer ceramics: a review, Prog. Nucl. Energy 169 (2024) 105106, https://doi.org/10.1016/j.pnucene.2024.105106.
[12] S.S. Hossain, P.K. Roy, C.-J. Bae, Utilization of waste rice husk ash for sustainable geopolymer: a review, Constr. Build. Mater. 310 (2021) 125218, https://doi.org/10.1016/j.conbuildmat.2021.125218.
[13] Z. Moujoud, S. Sair, H. Ait Ousaleh, I. Ayouch, A. El Bouari, O Tanane, Geopolymer composites reinforced with natural Fibers: a review of recent advances in processing and properties, Constr. Build. Mater. 388 (2023) 131666, https://doi.org/10.1016/j.conbuildmat.2023.131666.
[14] Z. Bian, J.-X. Lu, Y. Huang, D. Xuan, G. Ou, C. Sun Poon, Recycling of waste glass in lightweight geopolymer using incineration bottom ash as a foaming agent: towards energy conservation, Constr. Build. Mater. 400 (2023) 132632, https://doi.org/10.1016/j.conbuildmat.2023.132632.
[15] S. Panda, A. Nanda, S.K. Panigrahi, Potential utilization of waste plastic in sustainable geopolymer concrete production: a review, J. Environ. Manage. 366 (2024) 121705, https://doi.org/10.1016/j.jenvman.2024.121705.
[16] T. Lan, Y. Meng, T. Ju, Z. Chen, Y. Du, Y. Deng, et al., Synthesis and application of geopolymers from municipal waste incineration fly ash (MSWI FA) as raw ingredient - A review, Resour. Conserv. Recycl. 182 (2022) 106308, https://doi.org/10.1016/j.resconrec.2022.106308.
[17] N.B. Singh, B. Middendorf, Geopolymers as an alternative to Portland cement: an overview, Constr. Build. Mater. 237 (2020) 117455, https://doi.org/10.1016/J.CONBUILDMAT.2019.117455.
[18] T. Glasby, G.R. DJ, AJ, EFC geopolymer concrete aircraft pavements at Brisbane West Wellcamp Airport, Concrete (2015) 1–9.
[19] J. Davidovits, Years of successes and failures in geopolymer applications. Market trends and potential breakthroughs, Geopolymer 2002 Conference 28 (2002), 29–29.
[20] J. Davidovits, Geopolymers: man-made rock geosynthesis and the resulting development of very early high strength cement, Ournal. Mater. Educat. 16 (1994), 91–91.
[21] M.A. Al-Ghouti, M. Khan, M.S. Nasser, K. Al Saad, O.E Heng, Application of geopolymers synthesized from incinerated municipal solid waste ashes for the removal of cationic dye from water, PLoS One 15 (2020) e0239095, https://doi.org/10.1371/JOURNAL.PONE.0239095.
[22] Z. Yu, W. Song, P. Ding, Mesoporous geopolymer for improved adsorption and immobilization of copper ions, Desalination Water Treat 201 (2020) 278–288, https://doi.org/10.5004/dwt.2020.25926.
[23] Y. Pan, Y. Bai, C. Chen, S. Yao, Q. Tian, H. Zhang, Effect of calcination temperature on geopolymer for the adsorption of cesium, Mater. Lett. 330 (2023) 133355, https://doi.org/10.1016/j.matlet.2022.133355.
[24] T.W. Cheng, M.L. Lee, M.S. Ko, T.H. Ueng, S.F. Yang, The heavy metal adsorption characteristics on metakaolin-based geopolymer, Appl. Clay Sci. 56 (2012) 90–96, https://doi.org/10.1016/j.clay.2011.11.027.
[25] A.A. Siyal, M.R. Shamsuddin, M.I. Khan, N.E. Rabat, M. Zulfiqar, Z. Man, et al., A review on geopolymers as emerging materials for the adsorption of heavy metals and dyes, J. Environ. Manage. 224 (2018) 327–339, https://doi.org/10.1016/j.jenvman.2018.07.046.
[26] X. Qu, M. Tian, B. Liao, A Chen, Enhanced electrochemical treatment of phenolic pollutants by an effective adsorption and release process, Electrochim. Acta 55 (2010) 5367–5374, https://doi.org/10.1016/j.electacta.2010.04.089.
[27] N. Solomakou, A.M. Goula, Treatment of olive mill wastewater by adsorption of phenolic compounds, Rev. Environ. Sci. Biotechnol. 20 (2021) 839–863, https://doi.org/10.1007/s11157-021-09585-x.
[28] A. Arditsoglou, D. Voutsa, Partitioning of endocrine disrupting compounds in inland waters and wastewaters discharged into the coastal area of Thessaloniki, Northern Greece, Environ. Sci. Pollution Res. 17 (2010) 529–538, https://doi.org/10.1007/s11356-009-0172-y.
[29] M. Zhou, J. Zhang, C. Sun, Occurrence, ecological and human health risks, and seasonal variations of phenolic compounds in surface water and sediment of a potential polluted river basin in China, Int. J. Environ. Res. Public Health 14 (2017) 1140, https://doi.org/10.3390/ijerph14101140.
[30] Y. Pan, Y. Zhang, M. Hou, J. Xue, R. Qin, M. Zhou, et al., Properties of polyphenols and polyphenol-containing wastewaters and their treatment by Fenton/Fenton-like reactions, Sep. Purif. Technol. 317 (2023) 123905, https://doi.org/10.1016/j.seppur.2023.123905.
[31] R.K. Mishra, S.S. Mentha, Y. Misra, N. Dwivedi, Emerging pollutants of severe environmental concern in water and wastewater: a comprehensive review on current developments and future research, Water-Energy Nexus 6 (2023) 74–95, https://doi.org/10.1016/j.wen.2023.08.002.
[32] X. Song, C. Li, Z. Chai, Y. Zhu, Y. Yang, M. Chen, et al., Application of diatomite for gallic acid removal from molasses wastewater, Sci. Total Environ. 765 (2021) 142711, https://doi.org/10.1016/j.scitotenv.2020.142711.
[33] D. Wianowska, M. Olszowy-Tomczyk, A concise profile of gallic acid—from its natural sources through biological properties and chemical methods of determination, Molecules 28 (2023) 1186, https://doi.org/10.3390/molecules28031186.
[34] Y. Luo, G. Dao, G. Zhou, Z. Wang, Z. Xu, X. Lu, et al., Effects of low concentration of gallic acid on the growth and microcystin production of Microcystis aeruginosa, Sci. Total Environ. 916 (2024) 169765, https://doi.org/10.1016/j.scitotenv.2023.169765.
[35] S. Mamman, S.S. Abdullahi, A.H. Birniwa, O.D. Opaluwa, R.E.A. Mohammad, O. Okiemute, et al., Influence of adsorption parameters on phenolic compounds removal from aqueous solutions: a mini review, Desalination Water Treat 320 (2024) 100631, https://doi.org/10.1016/j.dwt.2024.100631.
[36] N. Mu'azu, N. Jarrah, M. Zubair, O. Alagha, Removal of phenolic compounds from water using sewage sludge-based activated carbon adsorption: a review, Int. J.

Environ. Res. Public Health 14 (2017) 1094, https://doi.org/10.3390/ijerph14101094.
[37] X. Jia, Y. Liu, Z. Yang, A. Zhang, P. Liu, Z. Liu, Construction of coal fly ash-based spherical grain adsorbents and their adsorption characteristics on phenolic compounds, Colloids and Surfaces C: Environ. Aspects 2 (2024) 100042, https://doi.org/10.1016/j.colsuc.2024.100042.
[38] T.A. Oyehan, F.A. Olabemiwo, B.S. Tawabini, T.A. Saleh, The capacity of mesoporous fly ash grafted with ultrathin film of polydiallyldimethyl ammonium for enhanced removal of phenol from aqueous solutions, J. Clean. Prod. 263 (2020) 121280, https://doi.org/10.1016/j.jclepro.2020.121280.
[39] D.A. Hijazi, A. BiBi, M.A Al-Ghouti, Sustainable waste utilization: geopolymeric fly ash waste as an effective phenol adsorbent for environmental remediation, Resour., Environ. Sustain. 15 (2024) 100142, https://doi.org/10.1016/j.resenv.2023.100142.
[40] Sogama. El Complejo Medioambiental de Cerceda 2023. https://www.sogama.gal/es/el-complejo-medioambiental-de-cerceda (accessed March 26, 2024).
[41] H. Jin, Y. Zhang, Q. Wang, Q. Chang, C. Li, Rapid removal of methylene blue and nickel ions and adsorption/desorption mechanism based on geopolymer adsorbent, Colloid. Interface Sci. Commun. 45 (2021) 100551, https://doi.org/10.1016/j.colcom.2021.100551.
[42] İ. Kara, D. Yilmazer, S.T. Akar, Metakaolin based geopolymer as an effective adsorbent for adsorption of zinc(II) and nickel(II) ions from aqueous solutions, Appl. Clay Sci. 139 (2017) 54–63, https://doi.org/10.1016/j.clay.2017.01.008.
[43] N.B. Singh, B. Middendorf, Geopolymers as an alternative to Portland cement: an overview, Constr. Build. Mater. 237 (2020) 117455, https://doi.org/10.1016/j.conbuildmat.2019.117455.
[44] B. Aouan, M. El Alouani, S. Alehyen, M. Fadil, H. Saufi, A. Laghzizil, et al., Application of central composite design for optimisation of the development of metakaolin based geopolymer as adsorbent for water treatment, Int. J. Environ. Anal. Chem. 104 (2024) 2623–2641, https://doi.org/10.1080/03067319.2022.2070010.
[45] N. Ariffin, M.M.A.B. Abdullah, P. Postawa, S. Zamree Abd Rahim, M.R.R. Mohd Arif Zainol, R. Putra Jaya, et al., Effect of aluminium powder on kaolin-based geopolymer characteristic and removal of Cu2+, Materials (Basel) 14 (2021) 814, https://doi.org/10.3390/ma14040814.
[46] J.L. Diaz de Tuesta, A. Quintanilla, D. Moreno, V.R. Ferro, J.A. Casas, Simulation and optimization of the CWPO process by combination of aspen plus and 6-factor doehlert matrix: towards autothermal operation, Catalysts 10 (2020) 548, https://doi.org/10.3390/catal10050548.
[47] L. Li, S. Wang, Z. Zhu, Geopolymeric adsorbents from fly ash for dye removal from aqueous solution, J. Colloid Interface Sci. 300 (2006) 52–59, https://doi.org/10.1016/J.JCIS.2006.03.062.
[48] A.A. Siyal, M.R. Shamsuddin, N.E. Rabat, M. Zulfiqar, Z. Man, A. Low, Fly ash based geopolymer for the adsorption of anionic surfactant from aqueous solution, J. Clean. Prod. 229 (2019) 232–243, https://doi.org/10.1016/J.JCLEPRO.2019.04.384.
[49] X. Feng, S. Yan, S. Jiang, K. Huang, X. Ren, X. Du, et al., Green synthesis of the metakaolin/slag based geopolymer for the effective removal of methylene blue and Pb (II), silicon 14 (2022) 6965–6979, https://doi.org/10.1007/S12633-021-01439-Z/METRICS.
[50] M. Król, J. Minkiewicz, W. Mozgawa, IR spectroscopy studies of zeolites in geopolymeric materials derived from kaolinite, J. Mol. Struct. 1126 (2016) 200–206, https://doi.org/10.1016/J.MOLSTRUC.2016.02.027.
[51] L. Panda, S.S. Rath, D.S. Rao, B.B. Nayak, B. Das, P.K. Misra, Thorough understanding of the kinetics and mechanism of heavy metal adsorption onto a pyrophyllite mine waste based geopolymer, J. Mol. Liq. 263 (2018) 428–441, https://doi.org/10.1016/J.MOLLIQ.2018.05.016.
[52] Davidovits J. Geopolymer Chemistry and Applications. 2008, vol. 171. 208AD.
[53] J. Xu, M. Li, D. Zhao, G. Zhong, Y. Sun, X. Hu, et al., Research and application progress of geopolymers in adsorption: a review, Nanomaterials 12 (2022) 3002, https://doi.org/10.3390/nano12173002.
[54] N. Toniolo, A. Rincón, J.A. Roether, P. Ercole, E. Bernardo, A.R. Boccaccini, Extensive reuse of soda-lime waste glass in fly ash-based geopolymers, Constr. Build. Mater. 188 (2018) 1077–1084, https://doi.org/10.1016/j.conbuildmat.2018.08.096.
[55] D.A. Hijazi, A. BiBi, M.A Al-Ghouti, Sustainable waste utilization: geopolymeric fly ash waste as an effective phenol adsorbent for environmental remediation, Resour., Environ. Sustain. 15 (2024) 100142, https://doi.org/10.1016/j.resenv.2023.100142.
[56] J. Liu, G. Xie, Z. Wang, Z. Li, X. Fan, H. Jin, et al., Synthesis of geopolymer using municipal solid waste incineration fly ash and steel slag: hydration properties and immobilization of heavy metals, J. Environ. Manage. 341 (2023) 118053, https://doi.org/10.1016/j.jenvman.2023.118053.
[57] B. Ren, Y. Zhao, H. Bai, S. Kang, T. Zhang, S. Song, Eco-friendly geopolymer prepared from solid wastes: a critical review, Chemosphere 267 (2021) 128900, https://doi.org/10.1016/j.chemosphere.2020.128900.
[58] A. Fernández-Jiménez, A. Palomo, Composition and microstructure of alkali activated fly ash binder: effect of the activator, Cem. Concr. Res. 35 (2005) 1984–1992, https://doi.org/10.1016/J.CEMCONRES.2005.03.003.
[59] K. Khatib, H. Kerroumi, M El Azhari, Synthesis, characterization and optimization of new adsorbent materials based on industrial discharges for the decontamination of liquid effluents, Mater Today Proc 22 (2020) 120–125, https://doi.org/10.1016/J.MATPR.2019.08.120.
[60] J. Yu, F. Ji, Q. Lv, W. Li, Z. Lin, Y. Peng, Mechanical property and microstructure of fly ash-based geopolymer by calcium activators, Case Studies in Construct. Mater. 21 (2024) e03811, https://doi.org/10.1016/j.cscm.2024.e03811.
[61] M. Yadav, L. Kumar, V. Yadav, K. Jagannathan, V.N. Singh, S.P. Singh, et al., Optimizing the Fly Ash/Activator ratio for a fly ash-based geopolymer through a study of microstructure, thermal stability, and electrical properties, Ceramics 6 (2023) 2352–2366, https://doi.org/10.3390/ceramics6040144.
[62] A.A. Siyal, R. Shamsuddin, A. Low, A. Hidayat, Adsorption kinetics, isotherms, and thermodynamics of removal of anionic surfactant from aqueous solution using fly ash, Water Air. Soil. Pollut. 231 (2020) 1–13, https://doi.org/10.1007/S11270-020-04879-2/FIGURES/5.
[63] E. Azhari, M. Synthesis, A. Karamanov, K. Khatib, L. Lahmyed, M El Azhari, Synthesis, characterization, and application of Geopolymer/TiO2 nanoparticles composite for efficient removal of Cu(II) and Cd(II) ions from aqueous media, Minerals 12 (2022) 1445, https://doi.org/10.3390/MIN12111445. Vol 12, Page 1445 2022.
[64] O. Shee-Ween, H. Cheng-Yong, L. Yun-Ming, M.M.A.B. Abdullah, H. Li Ngee, L.W. L. Chan, et al., Cold-pressed fly ash geopolymers: effect of formulation on mechanical and morphological characteristics, J. Mater. Res. Technol. 15 (2021) 3028–3046, https://doi.org/10.1016/j.jmrt.2021.09.084.
[65] U. Javed, F.U.A. Shaikh, P.K. Sarker, A comprehensive micro-nano investigative approach to study the development of aluminosilicate gel in binary blends of lithium slag geopolymer, Cem. Concr. Compos. 145 (2024) 105338, https://doi.org/10.1016/j.cemconcomp.2023.105338.
[66] S. Nenadović, J. Gulicovski, M. Mirković, L. Kljajević, I. Bošković, M. Vukčević, et al., Structural, mechanical and chemical properties of low content carbon geopolymer, Sustainability 14 (2022) 4885, https://doi.org/10.3390/su14094885.
[67] P. He, M. Wang, S. Fu, D. Jia, S. Yan, J. Yuan, et al., Effects of Si/Al ratio on the structure and properties of metakaolin based geopolymer, Ceram. Int. 42 (2016) 14416–14422, https://doi.org/10.1016/j.ceramint.2016.06.033.
[68] O.Y. Chén, J.S. Bodelet, R.G. Saraiva, H. Phan, J. Di, G. Nagels, et al., The roles, challenges, and merits of the p value, Patterns 4 (2023) 100878, https://doi.org/10.1016/j.patter.2023.100878.
[69] Y. Liu, C. Yan, Z. Zhang, H. Wang, S. Zhou, W. Zhou, A comparative study on fly ash, geopolymer and faujasite block for Pb removal from aqueous solution, Fuel 185 (2016) 181–189, https://doi.org/10.1016/J.FUEL.2016.07.116.
[70] E. Gökırmak Söğüt, M Gülcan, Adsorption: basics, properties, and classification, Adsorption through Adv. Nanoscale Mater. (2023) 3–21, https://doi.org/10.1016/B978-0-443-18456-7.00001-8. Elsevier.
[71] Q. Tian, K. Sasaki, Application of fly ash-based geopolymer for removal of cesium, strontium and arsenate from aqueous solutions: kinetic, equilibrium and mechanism analysis, Water Sci. Technol. 79 (2019) 2116–2125, https://doi.org/10.2166/WST.2019.209.
[72] J. Qiu, Y. Zhao, J. Xing, X. Sun, Fly ash-based geopolymer as a potential adsorbent for Cr(VI) removal, Desalination Water Treat 70 (2017) 201–209, https://doi.org/10.5004/DWT.2017.20493.
[73] Y.S. Ho, J.F. Porter, G. McKay, Equilibrium isotherm studies for the sorption of divalent metal ions onto peat: copper, nickel and lead single component systems, Water Air Soil Pollut. 141 (2002) 1–33, https://doi.org/10.1023/A:1021304828010/METRICS.
[74] K. Liang, X.Q. Wang, C.L. Chow, D. Lau, A review of geopolymer and its adsorption capacity with molecular insights: a promising adsorbent of heavy metal ions, J. Environ. Manage. 322 (2022) 116066, https://doi.org/10.1016/j.jenvman.2022.116066.
[75] O. Acisli, I. Acar, A. Khataee, Preparation of a fly ash-based geopolymer for removal of a cationic dye: isothermal, kinetic and thermodynamic studies, J. Ind. Eng. Chem. 83 (2020) 53–63, https://doi.org/10.1016/j.jiec.2019.11.012.
[76] X. Zhang, X. Zhou, T.B. Moghaddam, F. Zhang, F. Otto, Synergistic effects of iron (Fe) and biochar on light-weight geopolymers when used in wastewater treatment applications, J. Clean. Prod. 322 (2021) 129033, https://doi.org/10.1016/j.jclepro.2021.129033.
[77] D. Wattanasiriwech, K. Yomthong, S. Wattanasiriwech, Adsorption efficiency and photocatalytic activity of fly ash-based geopolymer foam mortar, Ceram. Int. 47 (2021) 27361–27371, https://doi.org/10.1016/j.ceramint.2021.06.158.
[78] A. Purbasari, D. Ariyanti, S. Sumardiono, K. Khairunnisa, T. Sidharta, Adsorption kinetics and isotherms of Cu(II) and Fe(II) ions from aqueous solutions by fly ash-based geopolymer, Chem. Chem. Technol. 16 (2022) 169–176, https://doi.org/10.23939/CHCHT16.02.169.
[79] Y. Zhang, L. Liu, Fly ash-based geopolymer as a novel photocatalyst for degradation of dye from wastewater, Particuology 11 (2013) 353–358, https://doi.org/10.1016/J.PARTIC.2012.10.007.
[80] N. Hasani, T. Selimi, A. Mele, V. Thaçi, J. Halili, A. Berisha, et al., Theoretical, equilibrium, kinetics and thermodynamic investigations of methylene blue adsorption onto lignite coal, Molecules 27 (2022) 1856, https://doi.org/10.3390/MOLECULES27061856, 2022, Vol 27, Page 1856.